



Evaluation of urban flood adaptability based on the InVEST model and GIS: A case study of New York City, USA

Song Yao^{1,2} · Guoping Huang³ · Zihan Chen⁴

Received: 24 July 2023 / Accepted: 15 April 2024 / Published online: 8 May 2024
© The Author(s), under exclusive licence to Springer Nature B.V. 2024

Abstract

Flood risk has become a serious challenge for many cities, including New York City (NYC). Evaluating urban flood adaptability evaluation is crucial for regulating storm and rain risks. In this study, we proposed an integrated framework based on the Integrated Valuation of Ecosystem Services (InVEST) model and Geographic Information System (GIS). First, the InVEST model was used to assess the water yield, soil conservation, and water quality purification in NYC. Second, the entropy weighting method was employed to determine the weights of indicators for computing the flood adaptability evaluation (FAE). Third, a spatial correlation of FAE was conducted and finally delineated the flood adaptability zones in GIS. The results show that: (1) The spatial distribution of FAE was uneven, high in the surrounding area and low in the center. (2) The Moran's I for FAE was 0.644, showing an overall positive spatial relationship of FAE. High-scoring clusters were located in the southeastern area while low-scoring clusters were in the northern, central, and southwestern areas. (3) The FAE in NYC can be divided into five categories: the lower-adapted zone (0.22–0.27), low-adapted zone (0.28–0.31), medium-adapted zone (0.32–0.36), high-adapted zone (0.37–0.43) and higher-adapted zone (0.44–0.50). These results of the study can provide evidence and recommendations for flood risk management in NYC and other cities worldwide.

Keywords Flood adaptability · InVEST model · Water yield · Soil conservation · Water quality purification · New York City

✉ Guoping Huang
guopingh@usc.edu

Song Yao
12312001@zju.edu.cn

¹ College of Civil Engineering and Architecture, Zhejiang University, Hangzhou 310058, China

² Department of Regional and Urban Planning, Zhejiang University, Hangzhou 310058, China

³ Spatial Sciences Institute, USC Dana and David Dornsife College of Letters, Arts and Sciences, University of Southern California, Los Angeles, CA 90089, USA

⁴ George School, Newtown, PA 18940, USA

1 Introduction

Floods are often considered to be the most common natural disaster worldwide (Stefanidis and Stathis 2013; Mojaddadi et al. 2017; Souissi et al. 2020) posing a serious threat to our socio-economic and population security (Boruff 2009; Hammond et al. 2015). From 2000 to 2019, floods caused an estimated \$651 billion of losses worldwide (UNDRR 2020; Tellman et al. 2021), posing a significant threat to the sustainable development of cities (Tellman et al. 2021; Hallegatte et al. 2017). With climate change and population growth, the risk of rainstorm-induced flooding is expected to increase in the future (Rufat and Botzen 2022; Boulange et al. 2021; Hammond et al. 2015), making flood risk management an important challenge facing many cities (Mojaddadi et al. 2017).

Sustainable urban flood management has garnered widespread attention as a solution to urban flood risk (Pour et al. 2020). In the US, many practitioners and researchers have proposed best management practices (Fletcher et al. 2015), low-impact development models (Pyke et al. 2011), and sustainable urban drainage systems (Mitchell 2005). In addition, blue-green infrastructure (Thorne et al. 2018), water-sensitive urban design (Morison and Brown 2011), and low-impact developments urban design (Voyde et al. 2010) were also widely advocated by researchers. However, these concepts and strategies are still in the development stage and have only been applied in small-scale environments such as experimental pilot projects and local areas (Nguyen et al. 2019). In recent years, the concept and practice of Sponge City have gained recognition as an effective means of managing rainstorm risk (Shao et al. 2019; Li et al. 2019). Sponge cities prioritize enhancing the resilience of urban areas to rainstorm disasters by maximizing natural accumulation, infiltration, and purification of urban flood (Yu et al. 2015; Chen et al. 2022). Therefore, this study employed the flood adaptability evaluation (FAE) to assess urban flood risk based on the principles of Sponge City.

Conducting scientific assessments of flood risk is a prerequisite and foundation for implement sustainable urban flood management (Chen et al. 2022; Zhang et al. 2022). In recent years, many scholars have conducted extensive research at the global (Ward et al. 2013), national (Zhao et al. 2014), regional (Sun et al. 2020), provincial (Ji and Chen 2022), and city levels (Chen et al. 2015). In general, there are three approaches to assessing flood risk (Xu et al. 2018): (1) Historical disaster statistics method. This method relies on analyzing historical flood data to evaluate current flood risk through mathematical analysis (Luu et al. 2019). For example, Zhao et al. conducted a flood risk evaluation in mainland China based on historical hazard data (Zhao et al. 2014), and Adikari et al. used historical flood data to assess the flood vulnerability of selected megacities in Asia (Adikari et al. 2010). However, typically lack spatial resolution beyond the county and city scale, thus hindering accurate identification of spatial characteristics of flood risk (Xu et al. 2018). (2) Scenario simulation. This method employs hydrodynamic models to simulate flood risk under different scenarios, providing an intuitive depiction of flood characteristics (Willems 2013). For example, Wang et al. assessed the flood resilience of urban drainage systems based on scenario simulation (Wang et al. 2021), and Wang et al. modeled surface flooding under different scenarios to assess flood resilience at the urban drainage catchment scale (Wang et al. 2019). However, in scenario modeling, parameter preparation and calibration are time-consuming, and data accuracy requirements are high, which limits the applicability of this method (Hong et al. 2018). (3) Multi-criteria analysis. This method calculates flood risk by studying the causes and formation mechanisms of flood disasters, constructing

a multi-indicator system, and assigning weights to the indicators. This method is simple to operate, has a low demand for data, and is widely used (Cai et al. 2021). For example, Sun et al. constructed a flood disaster risk assessment system with three criteria: hazard intensity, exposure, and urban adaptability (Sun et al. 2020), and Yang et al. constructed a flood vulnerability indicator system based on exposure, sensitivity, and adaptability (Yang et al. 2018). However, there are no standardized criteria for the selection of assessment indicators, and most of the studies reveal only temporal variations, with few studies revealing the spatial characteristics of flood risk, which may lead to weaker guidance for specific practices (Cai et al. 2021). Given the limitations of these three methods, there is a need to innovate and develop new approaches to bolster flood management efforts.

In recent years, there has been a new emergence of geographic information system (GIS)-based approaches in flood risk evaluation (Tayyab et al. 2021; Cabrera and Lee 2020; Lyu et al. 2018). The method collects and processes a variety of data, including meteorological data, geographic information data, and socio-economic data, to create a visual flood risk map, that shows the spatial characteristics of floods. It effectively addresses the shortcomings of traditional methods regarding visualization and data availability. Therefore, this study integrated the multi-criteria analysis with GIS to develop a comprehensive multi-indicator system for FAE. Leveraging the Integrated Valuation of Ecosystem Services and Tradeoffs (InVEST) model, we can assess and visually represent the natural resources and services crucial for sustaining human livelihoods. It helps explore how changes in ecosystems affect the flow of diverse socio-economic processes (Sharp et al. 2018). Using the InVEST model for FAE can enhance our understanding of hydrological cycling processes. In selecting evaluation indicators, it is important to consider the different surface runoff generated by rainfall at various magnitudes, which have different impacts on urban environments, ecosystems, water resources, and water safety, and thus should affect the measures and hydrological control indicators for urban flood management. Therefore, this study referred to the hydrological control indicators commonly used in various US states (Atlanta Regional Commission 2016; District of Columbia, Department of Environment 2020; New York Division of Engineering 2016; The Minnesota Stormwater Steering Committee 2013; Wisconsin Department of Natural Resources 2017). Based on the current widely adopted concept of total runoff control, three control indicators, namely infiltration, stream power erosion, and non-point source pollution (Goyen et al. 2012), were selected. In addition, the entropy method was used to determine the indicator weights, and the GIS was used to visualize the results of the urban flood adaptation evaluation.

New York City (NYC), the largest city in the United States, is highly vulnerable to flooding from coastal storms due to its intensively used waterfront and long coastline. Flood risk is expected to increase in the future with climate change and sea level rise. Therefore, there is an urgent need to conduct a flood risk assessment for NYC.

This study aimed to develop an integrated framework for FAE to support urban flood management using NYC as an example to evaluate its urban flood adaptability based on the InVEST model and GIS. There were three main objectives: (1) identifying the spatial distribution characteristics of FAE; (2) delineating the zones of FAE; and (3) proposing recommendations for sustainable urban flood management in New York City. The research results can support decision-making regarding flood risk management in NYC and other cities worldwide.

2 Study area and data

2.1 Study area

NYC is situated on the coastal plain at the mouth of the Hudson River in the northeastern United States, adjacent to the Atlantic Ocean. The city is comprised of five boroughs: Manhattan, Queens, Brooklyn, the Bronx, and Staten Island (Fig. 1).

NYC features a predominantly flat terrain, with the highest elevation found at Todt Hill on Staten Island at approximately 124.9 m. The combination of rising sea levels, increased storm surges, and more frequent extreme precipitation events has heightened the risk of flooding in NYC because of its 520 miles of coastline and proximity to the Hudson River. On October 29, 2012, Hurricane Sandy brought devastating storm surges that inundated numerous streets, tunnels, and subway lines in downtown Manhattan and other areas, resulting in widespread power outages throughout the city and its suburbs. Monitoring assessments indicate that sea levels in New York have risen 1 foot (approximately 30 cm) over the past 100 years with projections indicating a future rise of 10 inches (about 25 cm) every 20 years. This further exposes vulnerable populations, and critical infrastructure facilities to climate risks. Therefore, it is imperative to evaluate NYC's flood adaptability to effectively address future urban flood risk.

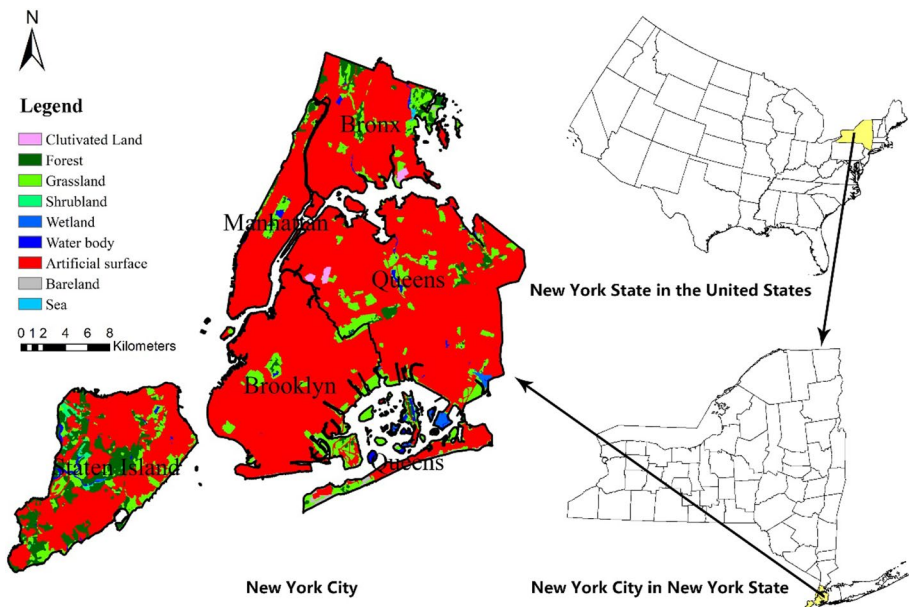



Fig. 1 Location of New York City

2.2 Data sources




The land cover data used in this study were obtained from GlobeLand30 2020 (Jun et al. 2014), with an overall precision of 85.72% and a Kappa coefficient of 0.82, indicating high interpretive precision. The administrative boundary and Digital Elevation Model (DEM) data for NYC were obtained from NYC Open Data (2013). Annual precipitation data from 1991 to 2020 were gained from the PRISM Climate Group (National Earth System Science Data Center 2023). Annual potential evapotranspiration Data were obtained from the Pant Science Data Center (Zomer et al. 2022). Plant Available Water Content data were gained from ISRIC's SoilGrids 2017 Available Water Content (AWC) (Shangguan et al. 2017), and the AWC layer for 7 soil depth intervals provided by the data set was calculated by weighted averaging. Root restricting layer depth data for soil were obtained from the Land–Atmosphere Interaction Research Group at Sun Yat-sen University of China (Shangguan et al. 2017). Watershed data were obtained from The HydroBASINS database (Lehner and Grill 2013), and soil data were obtained from the Harmonized World Soil Database v 1.2 (FAO Soils Portal 2008). The types, spatial resolutions, and sources of the data are presented in Table 1. The biophysical table required for calculating water yield, soil conservation, and water quality purification can be found in the Supplementary Material. All data were projected into the WGS 1984 UTM Zone N18 coordinate system using ArcGIS Desktop 10.2 and resampled to a 30m resolution.

3 Methods

3.1 Research framework

The research framework is shown in Fig. 2. More details can be found in the following sections.

3.2 Indicator selection and calculation



The InVEST model is an ecosystem service assessment model, designed to analyze how alterations in ecosystems may impact the benefits received by people (Sharp et al. 2018). In the United States, hydrological control indicators are commonly divided into six categories, including infiltration, non-point source pollution, stream power erosion, minor flooding, extreme flood marks, and emergency evacuation control indicators (Atlanta Regional Commission 2016; District of Columbia, Department of Environment 2020; New York Division of Engineering 2016; The Minnesota Stormwater Steering Committee 2013; Wang et al. 2015a, b; Wisconsin Department of Natural Resources 2017). Based on the widely adopted concept of total runoff control, this study selected infiltration, stream power erosion, and non-point source pollution as the control indicators (Goyen et al. 2012), and we used the Annual Water Yield, Sediment Delivery Ratio, and Nutrient Delivery Ratio modules of the InVEST model to calculate the water yield, soil conservation and water quality purification.

Table 1 Data source

Data	Resolution	SOURCE
Administrative boundary		https://opendata.cityofnewyork.us/ (accessed on 17 December 2022)
Land cover	30 m	http://globeland30.org/ (accessed on 24 December 2022)
DEM	1ft	https://opendata.cityofnewyork.us/ (accessed on 17 December 2022)
Annual precipitation	800 m	https://prism.oregonstate.edu/ (accessed on 10 April 2023)
Potential evapotranspiration	30"	https://www.plantplus.cn/cn/dataset/1512D26417FF6A38 (accessed on 26 December 2022)
Plant available water content	250 m	https://data.isric.org/geonetwork/srv/eng/catalog.search#/metadata/e33e75c0-d9ab-46b5-a915-cb344345099c (accessed on 24 December 2022)
Root restricting layer depth	250 m	http://globalchange.bnu.edu.cn/research/dtb.jsp (accessed on 26 February 2023)
Watersheds	/	https://www.hydrosheds.org/products/hydrobasins (accessed on 24 December 2022)
Soil data	30"	https://www.fao.org/soils-portal/data-hub/soil-maps-and-databases/harmonized-world-soil-database-v12/en/ (accessed on 26 February 2023)

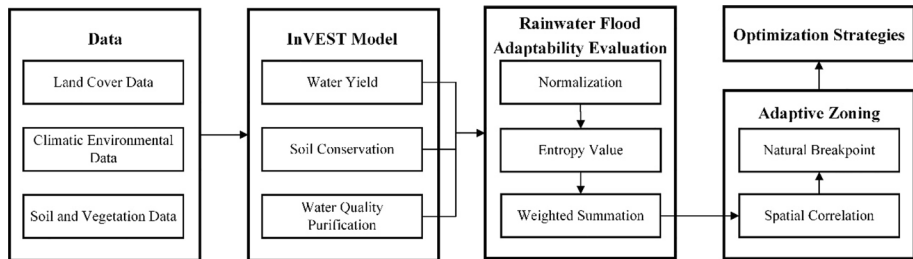


Fig.2 Research Framework

3.2.1 Water yield

The Annual Water Yield module in the InVEST model uses the Budyko Hypothesis, which is a water-heat coupling balance equation, to calculate the average annual water yield at the pixel scale (Sharp et al. 2018; Xu et al. 2013; Donohue et al. 2012). The water yield for each grid cell is obtained by subtracting the annual actual evapotranspiration from the annual precipitation. The formulae for calculating the water yield are as follows:

$$Y_i = \left(1 - \frac{AET_i}{P_i}\right) P_i \quad (1)$$

$$\frac{AET_i}{P_i} = \frac{1 + w_i R_i}{1 + w_i R_i + \left(\frac{1}{R_i}\right)} \quad (2)$$

$$w_i = Z \frac{AWC_i}{P_i} \quad (3)$$

$$R_i = \frac{k_i \times ET_{0i}}{P_i} \quad (4)$$

where Y_i represents the water yield (mm) for grid i ; P_i represents the annual precipitation (mm) for grid i ; AET_i represents the annual actual evapotranspiration (mm) for grid i ; R_i represents the Budyko dryness index for grid i ; w_i represents the ratio of vegetation effective water content to annual precipitation for grid i ; Z is a seasonal constant (ZHANG coefficient) (Zhang et al. 2012) used to characterize the seasonal features of precipitation; AWC_i represents the vegetation available water content (mm) for grid i ; k_i represents the vegetation transpiration coefficient for grid i ; ET_{0i} represents the reference evapotranspiration (mm) for grid i .

3.2.2 Soil conservation

The Sediment Delivery Ratio Module in InVEST (Sharp et al. 2018) is used to simulate soil conservation. Soil conservation is the potential soil erosion minus actual erosion at the grid unit level. The potential soil erosion is the soil erosion amount of bare land RKLS, and

the actual soil erosion is the erosion amount under natural conditions (USLE). They are calculated as follows:

$$RKLS_i = R_i \times K_i \times LS_i \quad (5)$$

$$USLE_i = R_i \times K_i \times LS_i \times P_i \times C_i \quad (6)$$

$$SR_i = RKLS_i - USLE_i \quad (7)$$

where Y_i is Where R_i is the rainfall erosion force factor of grid i [$\text{MJ}\cdot\text{mm}/(\text{hm}^2\cdot\text{h})$]; K_i is the soil erodibility factor of grid i [$\text{t}\cdot\text{h}/(\text{MJ}\cdot\text{mm})$]; LS_i is the terrain factor of grid i ; C_i is the vegetation cover factor of grid i ; P_i is the soil and water conservation measure factor of grid i ; and SR_i is the soil conservation quantity [t/hm^2] of grid i . R_i , the rainfall erosion force factor, is calculated according to the "Guidelines for Calculating Soil Loss of Production and Construction Projects SL773-2018" (Ministry of Water Resources of the People's Republic of China 2018). K_i is calculated using the method by Williams and Arnold (1997). LS_i is obtained by focal analysis of DEM in the ArcGIS. C_i and P_i are obtained based on the model description and reference literature (Sharp et al. 2018; Rao et al. 2013). The calculation formulae are as follows:

$$R_i = 0.067R_{id}^{1.627} \quad (8)$$

$$K_i = 0.1317K_{iEPIC} \quad (9)$$

$$K_{iEPIC} = \left\{ 0.2 + 0.3 \exp \left[-0.0256SAN_i \left(1 - \frac{SIL_i}{100} \right) \right] \right\} \times \left(\frac{SIL_i}{CLA_i + SIL_i} \right)^{0.3} \\ \times \left(1 - \frac{0.25C_i}{C_i + \exp(3.72 - 2.95C_i)} \right) \\ \times \left(1 - \frac{0.7(1 - SAN_i/100)}{(1 - SAN_i/100) + \exp(22.9(1 - SAN_i/100) - 5.51)} \right) \quad (10)$$

where R_{id} is the multiannual average rainfall amount of grid i (mm), K_{iEPIC} is the K_i in the customary US units; SAN_i is the sand content (%) of grid i ; SIL_i is the silt content (%) of grid i ; CLA_i is the clay content (%) of grid i ; and C_i is the organic carbon content (%) of grid i . The data of SAN_i , SIL_i , CLA_i and C_i are from the World Soil Database.

3.2.3 Water quality purification

The Nutrient Delivery Ratio Module of the InVEST model is based on the mechanism by which vegetation and soil can transform or store ammonia and phosphorus pollutants in runoff, while ignoring other sources of pollution. The module uses the total amount of ammonia and phosphorus in the water to represent the water quality of a watershed (Sharp et al. 2018). A higher concentration of total ammonia and phosphorus indicates a greater degree of pollution in the watershed and a weaker water quality purification capacity. The calculation formula is as follows:

$$W_i = 1/A_i \quad (11)$$

$$A_i = H_i \times pol_i \quad (12)$$

$$H_i = \lambda_i / \lambda_j \quad (13)$$

$$\lambda_i = \log \left(\sum_U Y_u \right) \quad (14)$$

where W_i represents the water quality purification value for nutrient P in grid i ; A_i represents the pollutant load of P in grid i ; pol_i represents the output coefficient of P; H_i represents the hydrological sensitivity score; λ_i represents the runoff coefficient; λ_j represents the average runoff coefficient; and $\sum_U Y_u$ represents the sum of water yield in grid i and all grids that flow into grid i , respectively.

3.3 Calculation of indicator weights

The entropy weighting method is a widely used objective assignment method that eliminates subjective human bias (Shannon 1948). The method determines the indicator weight values based on the amount of information contained in the degree of data variability of each indicator, which is calculated by the following process:

Step 1 data normalization

Positive indicators:

$$V_{ij} = \frac{x_{ij} - x_{\min}}{x_{\max} - x_{\min}} \quad (15)$$

Negative indicators:

$$V_{ij} = \frac{x_{\max} - x_{ij}}{x_{\max} - x_{\min}} \quad (16)$$

Step 2 entropy value calculation of each indicator

$$E_j = -\frac{1}{\ln n} \sum_{i=1}^n p_{ij} \times \ln p_{ij} \quad (17)$$

Step 3: coefficient of variability calculation

$$g_j = 1 - E_j \quad (1 \leq j \leq m) \quad (18)$$

Step 4 weight calculation

$$\omega_j = \frac{g_j}{\sum_{j=1}^m g_j} \quad (1 \leq j \leq m) \quad (19)$$

where x represents the indicators in NYC, V_{ij} denotes the normalized result of the j -th indicator for the i -th grid, x_{ij} , x_{\min} , x_{\max} denotes the original value, the max value and the min value of the j -th indicator for the i -th grid. p_{ij} is the characteristic weight of the j -th

indicator for the i -th grid, E_j , g_j , and ω_j are the entropy value, coefficient of variability and weight value of the j -th indicator, respectively, m represents the number of the indicators.

3.4 Valuation of flood adaptability



The water production, soil conservation and water purification indicators, are normalized, weighted and summed to obtain the FAE. The calculation formula is as follows:

$$FAE_i = \sum_{j=1}^m W_j \cdot P_{ij} \quad (1 \leq j \leq m) \quad (20)$$

where FAE_i represents the FAE value for the i -th grid.

3.5 Spatial autocorrelation analysis



Spatial autocorrelation refers to the phenomenon that things are clustered due to their inter-related characteristics, resulting in the phenomenon that the closer things are in space, the more similar they are (Diniz-Filho et al. 2003; Anselin 1995; Getis and Ord 2010). In this study, we used Geoda to calculate Moran's I and Local Indicators of Spatial Association (LISA) index. The Moran's I index is used to reveal the overall trend and variability of spatial correlation of the observed variable in the entire study area. The LISA index is used to describe the spatial autocorrelation between a spatial unit and other spatial units within its neighborhood, and it can reveal the agglomeration of spatial elements in the study area. The calculation formulas are as follows:

$$I = \frac{n \sum_{i=1}^n \sum_{j=1}^n W_{ij} (x_i - \bar{x}) (x_j - \bar{x})}{\left(\sum_{i=1}^n \sum_{j=1}^n W_{ij} \right) \sum_{i=1}^n (x_i - \bar{x})^2} (i \neq j) \quad (21)$$

$$I_i = \frac{(x_i - \bar{x}) \sum_{j=1}^n W_{ij} (x_j - \bar{x})}{S^2} (i \neq j) \quad (22)$$

$$S^2 = \frac{1}{n} \sum_{i=1}^n (x_i - \bar{x})^2 \quad (23)$$

where n represents the number of spatial units in the study area, x_i and x_j represent the observed values of spatial units i and j , \bar{x} denotes the mean value of the observed values, w_{ij} is the spatial weight matrix.

4 Results

4.1 The spatial distribution of FAE

The water yield was calculated using the Annual Water Yield module of the InVEST model. Spatially, the water yield values were high on the east side and low on the west side.

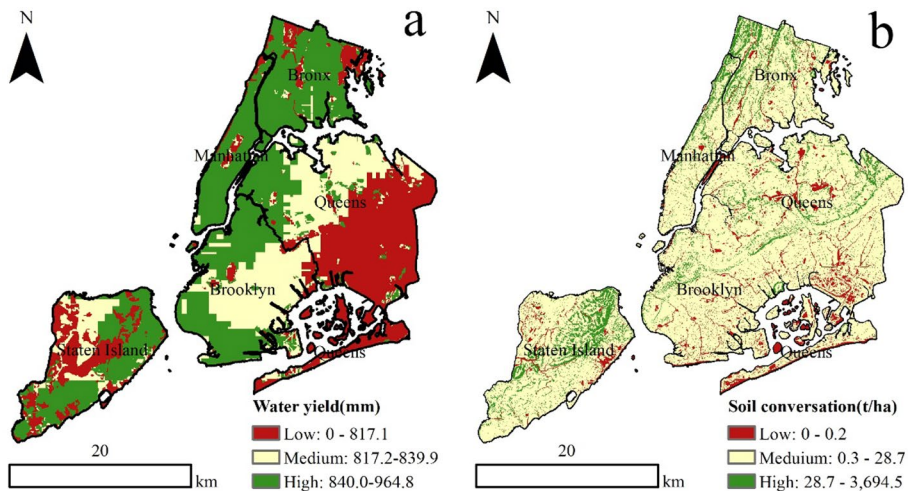


Fig. 3 Spatial distribution of **a** water yield and **b** soil conservation

High-value areas were mainly located in the Bronx, Staten Island, Brooklyn, and Manhattan. In contrast, the low-value areas were distributed in Staten Island and Queens (Fig. 3a). From the perspective of water balance, precipitation, and actual evapotranspiration are the two key factors determining the ecosystem water yield service. The spatial distribution pattern of water yield is closely related to the distribution patterns of annual precipitation and land cover types. Regions with high precipitation and low evapotranspiration (such as artificial surfaces) have stronger water yield capacity. In comparison, regions with low precipitation and high evapotranspiration (such as forests) have weaker water yield capacity.

We used the Sediment Delivery Ratio module of the InVEST model to calculate the soil conservation. The spatial pattern of soil conservation was high in the north and south while low in the middle. The high-value areas were mainly located in Staten Island, Manhattan, and Bronx, and the low-value areas were mainly located in Brooklyn and Queens (Fig. 3b). This may be closely related to the distribution patterns of land cover types. High soil conservation areas are mainly distributed in forests and grasslands, while low soil conservation areas are distributed on artificial surfaces.

The Nutrient Delivery Ratio module of the InVEST model was employed to assess the water quality purification capacity. The phosphorus export value was an indicator of the purification capacity, with larger outputs indicating poorer nitrogen and phosphorus purification capacity (Fig. 4a), so we took the inverse of the phosphorus export value and then normalized it to get the water purification capacity (Fig. 4b). The water quality purification pattern was characterized by a low middle and a high perimeter, with the high-value areas located in Staten Island and the low-value area predominantly located in Brooklyn, the Bronx and Queens.

The calculation of indicator weights based on the entropy weighting method was implemented in R4.3.2, the code of which can be found in the supplementary material. The weight values are shown in Table 2. The water yield, soil conservation, and water quality purification were normalized, weighted, and summed to obtain the FAE map (Fig. 5). The FAE showed a spatial distribution characteristic of low in the middle and high at the edges, with areas of high adaptability mainly concentrated in Staten Island and Manhattan, and

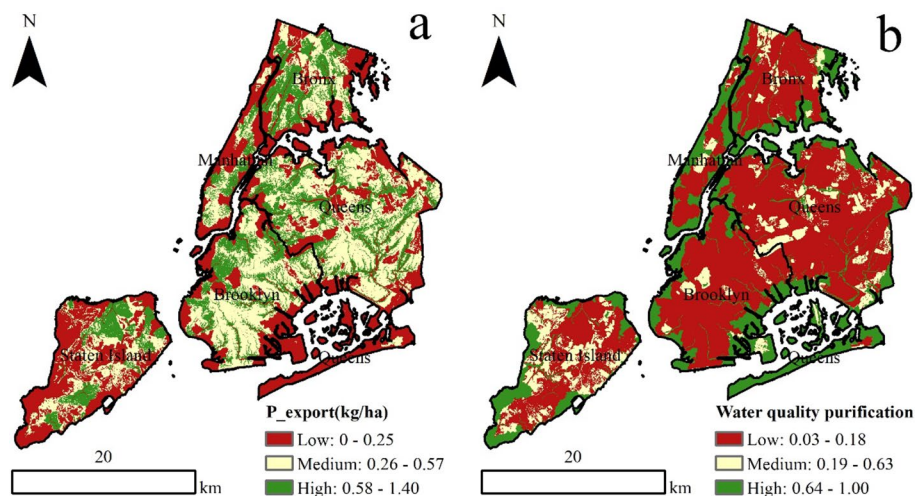


Fig. 4 Spatial distribution of **a** phosphorus export and **b** water quality purification

areas of low values mainly distributed in the Bronx, Brooklyn, and Queens. In terms of land cover types, the forest, grassland, and shrubland have high adaptability, and artificial surfaces have low adaptability.

4.2 Spatial correlation analysis of FAE

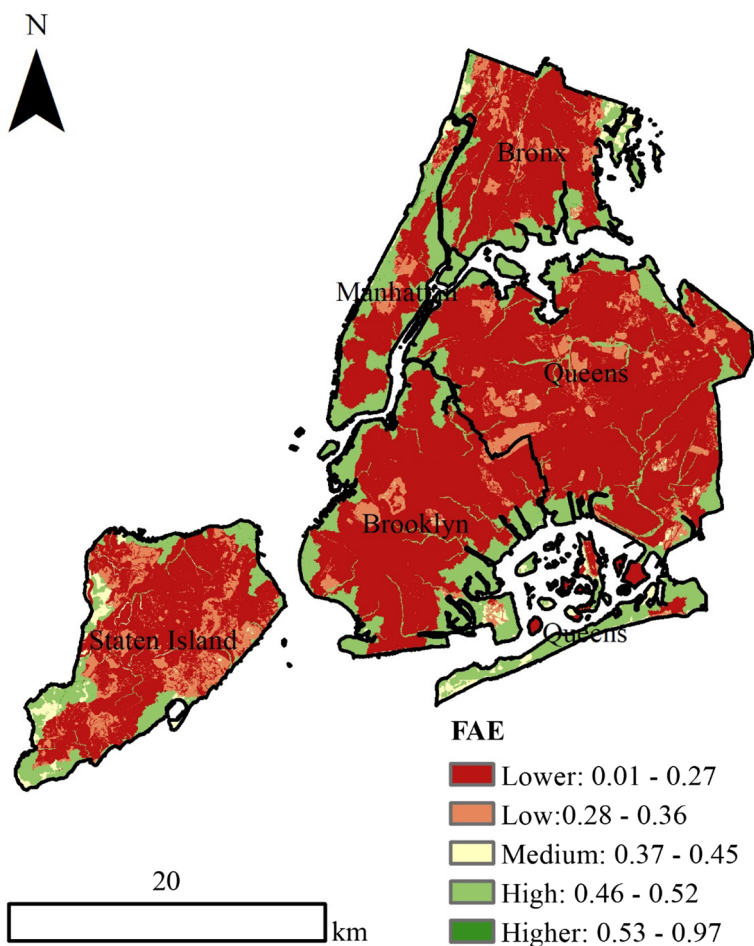
To avoid excessive fragmentation of the final partitioning results, we used the Create Fish-net tool in ArcGIS to convert the 30m grid to a more manageable spatial unit. Referring to previous studies (Winsemius et al. 2013; Ward et al. 2013; Xia et al. 2023; Feng et al. 2021), a 1 kilometer grid is considered to be a suitable spatial unit for management as it matches the size of a typical neighborhood.

From a global spatial correlation perspective (city scale), Moran's I, which stood at 0.644, indicating a positive spatial correlation as it surpassed 0. The Moran scatter plot (Fig. 6a) showed that most of the areas were located in the first quadrant (hot spot areas) and the third quadrant (cold spot areas), indicating that most areas exhibited strong positive spatial correlation. The spatial correlation characteristics of the FAE showed that high-value areas tended to be adjacent to high-value areas, and low-value areas tended to be adjacent to low-value areas.

From a local spatial correlation perspective (1 kilometer grid scale), the LISA cluster analysis (Fig. 6b) and Getis-Ord Gi* Analysis Chart (Fig. 7a) exhibited similarity in spatial distribution, indicating that high-high aggregation areas and hot spot areas of the FAE were mainly distributed in the southeast, where the FAE evaluation values were not only high but also concentrated and extensive. The low-low aggregation areas and cold spot areas of the FAE evaluation were mainly distributed in the Bronx, Brooklyn, Queens, and Staten Island in the north, central, and southwest regions, which have more artificial surfaces. Overall, the spatial distribution of the FAE was closely related to the land cover situation, with high-value

Table 2 The weight values of indicators

Indicators	Attribute	Weight
Water yield	+	0.2688
Soil conservation	+	0.4727
Water quality purification	+	0.2585

**Fig. 5** Spatial distribution of FAE in NYC

areas distributed in the southeast where there are fewer artificial surfaces and more ecological land, and low-value areas distributed in areas with high development intensity.

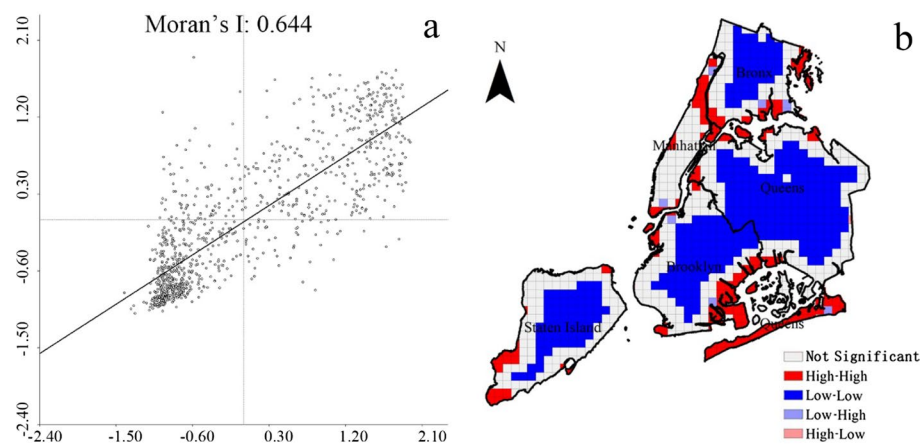


Fig. 6 **a** Moran scatter chart and **b** LISA agglomeration diagram

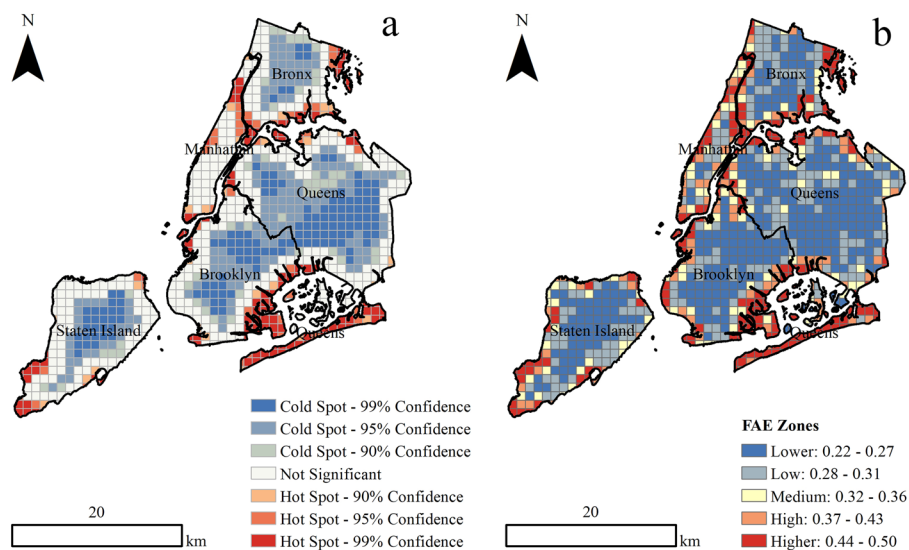



Fig. 7 **a** Analysis of cold and hot spots and **b** Zoning of FAE

Table 3 Percentage of different zones

F AE zones	Area (km ²)	Percentage
Lower	295.58	37.82
Low	233.30	29.85
Medium	53.47	6.84
High	78.93	10.10
Higher	120.22	15.39

4.3 Zoning of FAE




We used the natural breakpoint method to classify the FAE in NYC into five categories: the lower-adapted zone (0.22–0.27), low-adapted zone (0.28–0.31), medium-adapted zone (0.32–0.36), high-adapted zone (0.37–0.43) and higher-adapted zone (0.44–0.50) (Fig. 7b). Among them, the lower-adapted zone had the largest area of 295.58 km², accounting for 37.82% of the total area, and the high-adapted zone had the smallest area of 120.22 km², accounting for 15.39% (Table 3). In general, highly adapted zones were mainly concentrated on the edges, adjacent to water bodies and the ocean, while least adapted zones were mainly distributed on artificial surfaces.


5 Discussion

5.1 Recommendations for future development


This study may suggest avenues for improvement across multiple scales.



At the neighborhood scale, the clustering of lower-adapted zones indicated that these areas may benefit from individual improvement to enhance FAE adaptability precisely and intensively. Possible actions include protecting important buildings and building a local community that actively addresses the risk. Some short-term ways to prevent building damages from the flood are floodproofing and elevation of buildings (NYC Emergency Management 2014), while long-term solutions such as reducing impervious surface to trap, absorb rainwater, and reduce peak flow through retention, can be implemented in the community.



At the borough scale, addressing flood and rain risks in NYC could involve tacking features like the shoreline and the city center. The main risk along the shoreline arises from coastal storms, exemplified by Hurricane Sandy. Currently, NYC has designated Special Coastal Risk Districts in Queens and Staten Island to enhance resiliency (NYC Emergency Management 2014). For city centers that have shown low or lower adaptation due to their non-permeable ground, the expansion of sewer and drainage capacity may be a practical solution. However, it is important to note that nature-based solutions should be considered. Giving its permeable soil type beneath the pavement (Arup 2023), NYC stands out as an ideal candidate for employing these methods, facilitating improved drainage. An example of such nature-based solutions is NYC's investment in Right-Of-Way infrastructure, aiming to incorporate pervious surfaces like rain gardens onto streets and sidewalks to reduce storm runoff (NYC Environmental Protection 2022). Investing in preserving or building natural drainage corridors is also a cost-effective and ecologically favorable solution to managing stormwater, as evidenced by such projects in Staten Island (NYC Environmental Protection 2017).



At the city scale, the current situation could be improved by establishing policies to encourage green infrastructure, as well as funding the development of innovative approaches to flood management. Through the implementation of Special Risk Districts, policies could provide incentives and support for implementing green infrastructure such as rain gardens and green roofs. These policies may yield economic benefits, including increased property values due to reduced impact from heavy rain, and the creating of new employment in the green sector.

5.2 Possible directions for improvement



This study evaluated and mapped flood adaptability based on the InVEST model and GIS. However, the study has some limitations. First, the accuracy of the model results is directly affected by the quality of input data, such as land cover, precipitation, DEM, soil, and plant available water content. Some data used in this study were obtained from open-access websites with inadequate metadata regarding quality. Future research can improve the accuracy of evaluation results by collaborating with relevant departments to obtain authoritative data. Second, the InVEST model has a small number of parameters, and the selection of these parameters can greatly affect the accuracy of the results. The biophysical table used in this study was mainly obtained from a literature review (Allen et al. 2005; Hu et al. 2014; Li et al. 2014; Sharp et al. 2018; Wu et al. 2013), and there was a lack of local data from NYC. Further research can improve the model by obtaining more refined parameters specifically for the study area.

6 Conclusions

Research on sustainable urban flood management has been widely conducted around the world. However, although many studies have explored methods for assessing flood risk, few scholars have constructed evaluation indicators based on the principles of Sponge City.

In this study, we proposed an integrated framework based on the InVEST model and GIS to evaluate the urban flood adaptability in NYC. The following conclusions were obtained: (1) The spatial distribution of FAE was characterized by high in the surrounding area and low in the center. (2) The Moran's I for FAE was 0.644, showing an overall positive spatial relationship. High-scoring clusters were located in the southeastern area while low-scoring clusters were in the northern, central, and southwestern areas. (3) The FAE in NYC can be divided into five categories: the lower-adapted zone (0.22–0.27), low-adapted zone (0.28–0.31), medium-adapted zone (0.32–0.36), high-adapted zone (0.37–0.43) and higher-adapted zone (0.44–0.50). The results of the study can provide evidence and recommendations for flood risk management in NYC, and set an example of an evidence-based approach for other cities worldwide.

While meaningful findings were revealed through this study, several unresolved issues warrant further exploration and discussion in subsequent research. The indicators collected in this study may lack comprehensive due to constraints in data availability, suggesting the need for utilizing higher-quality data to construct a more thorough indicator system in future studies. Additionally, further research is warranted to explore strategies for mitigating flood risk.

Supplementary Information The online version contains supplementary material available at <https://doi.org/10.1007/s11069-024-06632-y>.

Acknowledgements This research was supported by the National Natural Science Foundation of China (Grant No. 51878593).

Author contributions Conceptualization, Song Yao and Zihan Chen; data curation, Song Yao; formal analysis, Song Yao and Zihan Chen; funding acquisition, Guoping Huang; methodology, Song Yao; resources, Guoping Huang; software, Song Yao; supervision, Guoping Huang; validation, Song Yao; visualization, Song Yao; writing—original draft preparation, Song Yao and Zihan Chen; writing—review and editing, Song Yao. All authors read and approved the final manuscript.

Funding This research was funded by the National Natural Science Foundation of China (Grant No. 51878593).

Data availability statement All the data used for the study appear in Sect. 2.2 of the submitted article.

Declarations

Conflict of interest The authors declare no conflicts of interest.

References

- Adikari Y, Osti R, Noro T (2010) Flood-related disaster vulnerability: an impending crisis of megacities in Asia. *J Flood Risk Manag* 3:185–191. <https://doi.org/10.1111/j.1753-318X.2010.01068.x>
- Allen RG, Pruitt WO, Raes D et al (2005) Estimating evaporation from bare soil and the crop coefficient for the initial period using common soils information. *J Irrig Drain Eng* 131:14–23. [https://doi.org/10.1061/\(ASCE\)0733-9437\(2005\)131:1\(14\)](https://doi.org/10.1061/(ASCE)0733-9437(2005)131:1(14))
- Anselin L (1995) Local indicators of spatial association—LISA. *Geogr Anal* 27:93–115. <https://doi.org/10.1111/j.1538-4632.1995.tb00338.x>
- Arup (2023) Arup GlobalSponge Cities Snapshot. <https://www.arup.com/perspectives/publications/research/section/global-sponge-cities-snapshot>. Accessed on 19 March 2023
- Atlanta Regional Commission (2016) Edition of the Georgia Stormwater Management Manual Volumes 1 & 2. <https://atlantaregional.org/natural-resources/water/georgia-stormwater-management-manual/>. Accessed on 19 March 2023
- Boruff BJ (2009) Environmental hazards: assessing risk and reducing disasters, 5th Edition – By Keith Smith and David N. Petley. *Geogr Res* 47:454–455. <https://doi.org/10.1111/j.1745-5871.2009.00611.x>
- Boulange J, Hanasaki N, Yamazaki D, Pokhrel Y (2021) Role of dams in reducing global flood exposure under climate change. *Nat Commun* 12:417. <https://doi.org/10.1038/s41467-020-20704-0>
- Cabrera JS, Lee HS (2020) Flood risk assessment for Davao Oriental in the Philippines using geographic information system-based multi-criteria analysis and the maximum entropy model. *J Flood Risk Manag* 13:e12607. <https://doi.org/10.1111/jfr3.12607>
- Cai S, Fan J, Yang W (2021) Flooding risk assessment and analysis based on GIS and the TFN-AHP method: a case study of Chongqing, China. *Atmosphere* 12:623. <https://doi.org/10.3390/atmos12050623>
- Chen Y, Zhou H, Zhang H et al (2015) Urban flood risk warning under rapid urbanization. *Environ Res* 139:3–10. <https://doi.org/10.1016/j.envres.2015.02.028>
- Chen Z, Mo C, Chen R, Peng B (2022) Assessment and zoning of rain and flood adaptability in the construction demonstration area of Sponge City in Changde City. *J Natl Resources* 37:2195–2208. <https://doi.org/10.31497/zrzyxb.20220818>. (in Chinese)
- Diniz-Filho JAF, Bini LM, Hawkins BA (2003) Spatial autocorrelation and red herrings in geographical ecology. *Glob Ecol Biogeogr* 12:53–64. <https://doi.org/10.1046/j.1466-822X.2003.00322.x>
- District of Columbia, Department of Environment (2020) Stormwater Management Guide Book. <https://doee.dc.gov/swguidebook>. Accessed on 19 March 2023
- Donohue RJ, Roderick ML, McVicar TR (2012) Roots, storms and soil pores: Incorporating key ecohydrological processes into Budyko's hydrological model. *J Hydrol* 436–437:35–50. <https://doi.org/10.1016/j.jhydrol.2012.02.033>
- FAO Soils Portal (2008) Harmonized World Soil Database v1.2. <https://www.fao.org/soils-portal/data-hub/soil-maps-and-databases/harmonized-world-soil-database-v12/en/>. Accessed on 19 March 2023
- Feng X, Jin X, Chen T, Wu J (2021) Understanding trade-offs and synergies of ecosystem services to support the decision-making in the Beijing–Tianjin–Hebei region. *Land Use Policy* 106:105446. <https://doi.org/10.1016/j.landusepol.2021.105446>
- Fletcher TD, Shuster W, Hunt WF et al (2015) SUDS, LID, BMPs, WSUD and more: the evolution and application of terminology surrounding urban drainage. *Urban Water J* 12:525–542. <https://doi.org/10.1080/1573062X.2014.916314>
- Getis A, Ord JK (2010) The analysis of spatial association by use of distance statistics. *Geogr Anal* 24:189–206. <https://doi.org/10.1111/j.1538-4632.1992.tb00261.x>

- Goyen AG, Lees SJ, Phillips BC (2012) Analysis of allotment based storage, infiltration and reuse drainage strategies to minimize urbanization effects. *Glob Solut Urban Drain* 1:17. [https://doi.org/10.1061/40644\(2002\)42](https://doi.org/10.1061/40644(2002)42)
- Hallegatte S, Vogt-Schilb A, Bangalore M, Rozenberg J (2017) *Unbreakable*. World Bank, Washington, DC
- Hammond MJ, Chen AS, Djordjević S et al (2015) Urban flood impact assessment: a state-of-the-art review. *Urban Water J* 12:14–29. <https://doi.org/10.1080/1573062X.2013.857421>
- Hong H, Panahi M, Shirzadi A et al (2018) Flood susceptibility assessment in Hengfeng area coupling adaptive neuro-fuzzy inference system with genetic algorithm and differential evolution. *Sci Total Environ* 621:1124–1141. <https://doi.org/10.1016/j.scitotenv.2017.10.114>
- Hu S, Cao M, Liu Q, Zhang T, Qiu H, Liu W, Song J (2014) Comparison of soil conservation functions of InVEST model from different perspectives. *Geogr Res* 33:2393–2406. <https://doi.org/10.11821/dljy201412016>. (in Chinese)
- Ji J, Chen J (2022) Urban flood resilience assessment using RAGA-PP and KL-TOPSIS model based on PSR framework: a case study of Jiangsu province, China. *Water Sci Technol* 86:3264–3280. <https://doi.org/10.2166/wst.2022.404>
- Jun C, Ban Y, Li S (2014) Open access to Earth land-cover map. *Nature* 514:434–434. <https://doi.org/10.1038/514434c>
- Lehner B, Grill G (2013) Global river hydrography and network routing: baseline data and new approaches to study the world's large river systems. *Hydrol Process* 27:2171–2186. <https://doi.org/10.1002/hyp.9740>
- Li T, Liu K, Hu S, Bao Y (2014) Evaluation of ecological benefits of soil loss and soil conservation in Qinling Mountains based on InVEST model. *Resources Environ the Yangtze River Basin* 23:1242–1250. <https://doi.org/10.11870/cjlyzyyhj201409009>. (in Chinese)
- Li Q, Wang F, Yu Y et al (2019) Comprehensive performance evaluation of LID practices for the sponge city construction: a case study in Guangxi, China. *J Environ Manage* 231:10–20. <https://doi.org/10.1016/j.jenvman.2018.10.024>
- Luu C, Von Meding J, Mojtahedi M (2019) Analyzing Vietnam's national disaster loss database for flood risk assessment using multiple linear regression-TOPSIS. *Int J Disaster Risk Reduct* 40:101153. <https://doi.org/10.1016/j.ijdr.2019.101153>
- Lyu H-M, Sun W-J, Shen S-L, Arulrajah A (2018) Flood risk assessment in metro systems of megacities using a GIS-based modeling approach. *Sci Total Environ* 626:1012–1025. <https://doi.org/10.1016/j.scitotenv.2018.01.138>
- Ministry of Water Resources of the People's Republic of China (2018) Announcement of the Ministry of Water Resources on Approving the Issuance of Three Water Conservancy Industry Standards, including the "Guidelines for the Calculation of Soil Loss in Production and Construction Projects". http://www.gov.cn/zhengce/zhengceku/2018-12/31/content_5440136.htm. Accessed on 19 March 2023
- Mitchell G (2005) Mapping hazard from urban non-point pollution: a screening model to support sustainable urban drainage planning. *J Environ Manage* 74:1–9. <https://doi.org/10.1016/j.jenvman.2004.08.002>
- Mojaddadi H, Pradhan B, Nampak H et al (2017) Ensemble machine-learning-based geospatial approach for flood risk assessment using multi-sensor remote-sensing data and GIS. *Geomat Nat Haz Risk* 8:1080–1102. <https://doi.org/10.1080/19475705.2017.1294113>
- Morison PJ, Brown RR (2011) Understanding the nature of publics and local policy commitment to Water Sensitive Urban Design. *Landsc Urban Plan* 99:83–92. <https://doi.org/10.1016/j.landurbplan.2010.08.019>
- National Earth System Science Data Center (2023). <http://www.geodata.cn/>. Accessed on 19 March 2023).
- New York Division of Engineering (2016) New York State Stormwater Management Design Manual. <https://www.dec.ny.gov/chemical/29072.html>. Accessed on 19 March 2023
- Nguyen TT, Ngo HH, Guo W et al (2019) Implementation of a specific urban water management: Sponge City. *Sci Total Environ* 652:147–162. <https://doi.org/10.1016/j.scitotenv.2018.10.168>
- NYC Emergency Management (2014) NYC'S Risk Landscape: A Guide to Hazard Mitigation. https://a860-gpp.nyc.gov/concern/nyc_government_publications/9306sz780. Accessed on 19 March 2023
- NYC Environmental Protection (2017) The Bluebelt Program. <https://www.nyc.gov/site/dep/water/the-bluebelt-program.page>. Accessed on 19 March 2023
- NYC Environmental Protection (2022) NYC green infrastructure 2021 annual report. https://a860-gpp.nyc.gov/concern/parent/bv73c3028/file_sets/qr46r355g. Accessed on 19 March 2023
- NYC Open Data (2013). <https://opendata.cityofnewyork.us/>. Accessed on 19 March 2023).

- Pour SH, Wahab AKA, Shahid S et al (2020) Low impact development techniques to mitigate the impacts of climate-change-induced urban floods: Current trends, issues and challenges. *Sustain Cities Soc* 62:102373. <https://doi.org/10.1016/j.scs.2020.102373>
- Pyke C, Warren MP, Johnson T et al (2011) Assessment of low impact development for managing storm-water with changing precipitation due to climate change. *Landsc Urban Plan* 103:166–173. <https://doi.org/10.1016/j.landurbplan.2011.07.006>
- Rao E, Xiao Y, Ouyang Z, Zheng H (2013) Spatial characteristics of soil conservation service and its impact factors in Hainan Island. *Acta Ecol Sin* 33:746–755. <https://doi.org/10.5846/stxb201203240400>. (in Chinese)
- Rufat S, Botzen WJW (2022) Drivers and dimensions of flood risk perceptions: revealing an implicit selection bias and lessons for communication policies. *Glob Environ Chang* 73:102465. <https://doi.org/10.1016/j.gloenvcha.2022.102465>
- Shangguan W, Hengl T, Mendes de Jesus J et al (2017) Mapping the global depth to bedrock for land surface modeling. *J Adv Model Syst* 9:65–88. <https://doi.org/10.1002/2016MS000686>
- Shao Z, Fu H, Li D et al (2019) Remote sensing monitoring of multi-scale watersheds impermeability for urban hydrological evaluation. *Remote Sens Environ* 232:111338. <https://doi.org/10.1016/j.rse.2019.111338>
- Sharp R, Tallis H T, Ricketts T et al. (2018) InVEST 3.12.0 User's Guide. <https://naturalcapitalproject.stanford.edu/software/invest>. Accessed on 26 November 2022
- Souissi D, Zouhri L, Hammami S et al (2020) GIS-based MCDM: AHP modeling for flood susceptibility mapping of arid areas, southeastern Tunisia. *Geocarto Int* 35:991–1017. <https://doi.org/10.1080/10106049.2019.1566405>
- Stefanidis S, Stathis D (2013) Assessment of flood hazard based on natural and anthropogenic factors using analytic hierarchy process (AHP). *Nat Hazards* 68:569–585. <https://doi.org/10.1007/s11069-013-0639-5>
- Sun S, Zhai J, Li Y et al (2020) Urban waterlogging risk assessment in well-developed region of Eastern China. *Phys Chem Earth Parts a/b/c* 115:102824. <https://doi.org/10.1016/j.pce.2019.102824>
- Tayyab M, Zhang J, Hussain M et al (2021) GIS-based urban flood resilience assessment using urban flood resilience model: a case study of Peshawar City, Khyber Pakhtunkhwa, Pakistan. *Remote Sens* 13:1864. <https://doi.org/10.3390/rs13101864>
- Tellman B, Sullivan JA, Kuhn C et al (2021) Satellite imaging reveals increased proportion of population exposed to floods. *Nature* 596:80–86. <https://doi.org/10.1038/s41586-021-03695-w>
- The Minnesota Stormwater Steering Committee (2013) The Minnesota Stormwater Manual. https://stormwater.pca.state.mn.us/index.php?title=Main_Page. Accessed on 19 March 2023
- Thorne CR, Lawson EC, Ozawa C et al (2018) Overcoming uncertainty and barriers to adoption of Blue-Green Infrastructure for urban flood risk management. *J Flood Risk Manag* 11:S960–S972. <https://doi.org/10.1111/jfr3.12218>
- UNDRR (2020) The Human Cost of Disasters: An Overview of the Last 20 Years (2000–2019). <https://www.undrr.org/publication/human-cost-disasters-overview-last-20-years-2000-2019>. Accessed on 13 March 2023
- Voyde E, Fassman E, Simcock R (2010) Hydrology of an extensive living roof under sub-tropical climate conditions in Auckland, New Zealand. *J Hydrol* 394:384–395. <https://doi.org/10.1016/j.jhydrol.2010.09.013>
- Wang H, Ding L, Cheng X, Li N (2015a) Hydrological control index system of urban stormwater management in the United States and its referential significance. *J Hydraul Eng* 46:1261–1271. <https://doi.org/10.1038/s41586-021-03695-w>. (in Chinese)
- Wang Z, Lai C, Chen X et al (2015b) Flood hazard risk assessment model based on random forest. *J Hydrol* 527:1130–1141. <https://doi.org/10.1016/j.jhydrol.2015.06.008>
- Wang Y, Feng F, Liu H et al (2019) Assessing catchment scale flood resilience of urban areas using a grid cell based metric. *Water Res* 163:114852. <https://doi.org/10.1016/j.watres.2019.114852>
- Wang M, Fang Y, Sweetapple C (2021) Assessing flood resilience of urban drainage system based on a 'do-nothing' benchmark. *J Environ Manage* 288:112472. <https://doi.org/10.1016/j.jenvman.2021.112472>
- Ward PJ, Jongman B, Weiland FS et al (2013) Assessing flood risk at the global scale: model setup, results, and sensitivity. *Environ Res Lett* 8:044019. <https://doi.org/10.1088/1748-9326/8/4/044019>
- Willems P (2013) Revision of urban drainage design rules after assessment of climate change impacts on precipitation extremes at Uccle, Belgium. *J Hydrol* 496:166–177. <https://doi.org/10.1016/j.jhydrol.2013.05.037>
- Williams JR, Arnold JG (1997) A system of erosion—sediment yield models. *Soil Technol* 11:43–55. [https://doi.org/10.1016/S0933-3630\(96\)00114-6](https://doi.org/10.1016/S0933-3630(96)00114-6)

- Winsemius HC, Van Beek LPH, Jongman B et al (2013) A framework for global river flood risk assessments. *Hydrol Earth Syst Sci* 17:1871–1892. <https://doi.org/10.5194/hess-17-1871-2013>
- Wisconsin Department of Natural Resources (2017) Non-Agricultural Revisions to Chapter NR 151, Runoff Management Rule. https://dnr.wi.gov/topic/stormwater/documents/NR151_non-ag_FS.pdf. Accessed on 19 March 2023
- Wu Z, Liu X, Liu B, Chu J, Pneg L (2013) Risk assessment of nitrogen and phosphorus loads in hainan island based on InVEST Model. *J Trop Crops* 34:1791–1797. [https://doi.org/10.3969/j.issn.1000-2561.2013.09.029\(inChinese\)](https://doi.org/10.3969/j.issn.1000-2561.2013.09.029(inChinese))
- Xia H, Yuan S, Prishchepov AV (2023) Spatial-temporal heterogeneity of ecosystem service interactions and their social-ecological drivers: implications for spatial planning and management. *Resour Conserv Recycl* 189:106767. <https://doi.org/10.1016/j.resconrec.2022.106767>
- Xu X, Liu W, Scanlon BR et al (2013) Local and global factors controlling water-energy balances within the Budyko framework. *Geophys Res Lett* 40:6123–6129. <https://doi.org/10.1002/2013GL058324>
- Xu H, Ma C, Lian J et al (2018) Urban flooding risk assessment based on an integrated k-means cluster algorithm and improved entropy weight method in the region of Haikou, China. *J Hydrol* 563:975–986. <https://doi.org/10.1016/j.jhydrol.2018.06.060>
- Yang W, Xu K, Lian J et al (2018) Integrated flood vulnerability assessment approach based on TOPSIS and Shannon entropy methods. *Ecol Ind* 89:269–280. <https://doi.org/10.1016/j.ecolind.2018.02.015>
- Yu K, Li D, Yuan H, Fu W, Qiao Q, Wang S (2015) “Sponge City”: theory and practice. *Urban Plan* 39:26–36. <https://doi.org/10.1181/cpr20150605a>. (in Chinese)
- Zhang C, Li W, Zhang B, Liu M (2012) Water Yield of Xitiaoxi River basin based on InVEST Modeling. *J Resources Ecol* 3:50–54. <https://doi.org/10.5814/j.issn.1674-764x.2012.01.008>
- Zhang K, Shalehy MH, Ezaz GT et al (2022) An integrated flood risk assessment approach based on coupled hydrological-hydraulic modeling and bottom-up hazard vulnerability analysis. *Environ Model Softw* 148:105279. <https://doi.org/10.1016/j.envsoft.2021.105279>
- Zhao Y, Gong Z, Wang W, Luo K (2014) The comprehensive risk evaluation on rainstorm and flood disaster losses in China mainland from 2004 to 2009: based on the triangular gray correlation theory. *Nat Hazards* 71:1001–1016. <https://doi.org/10.1007/s11069-013-0698-7>
- Zomer RJ, Xu J, Trabucco A (2022) Version 3 of the global aridity index and potential evapotranspiration database. *Sci Data* 9:409. <https://doi.org/10.1038/s41597-022-01493-1>

Publisher's Note Springer Nature remains neutral with regard to jurisdictional claims in published maps and institutional affiliations.

Springer Nature or its licensor (e.g. a society or other partner) holds exclusive rights to this article under a publishing agreement with the author(s) or other rightsholder(s); author self-archiving of the accepted manuscript version of this article is solely governed by the terms of such publishing agreement and applicable law.